Seal failure assessment of a major gas field via integration of seal properties and leakage phenomena

M. Foschi[1]* and J.A. Cartwright[1]
[1]Shell Geoscience Laboratory - Department of Earth Science, University of Oxford, South Parks Road, Oxford OX1 3AN, UK

*martinof@earth.ox.ac.uk

Acknowledgments

We thank the National Offshore Petroleum Titles Administrator (NOPTA) for the free access to seismic data, well data and reports. We are grateful with Schlumberger for providing software support. We thank Andy Aplin and Bruce Levell for discussion on seal capacity and leakage. We also thank Matteo Paganoni and James King for their constructive discussions and comments on an earlier version of the manuscript. We thank Elena Konstantinovskaya, Robert Locklair, Kurt Rudolph, and Hanneke Verweij for their invaluable reviews and for helping to improve this manuscript significantly.

Abstract

We present a seismic and well-based interpretation of a large 'leakage zone' above the Scarborough Gas Field, Exmouth Plateau, NW shelf of Australia. This leakage zone, well imaged on 3-D seismic, extends over a region of 100 km^2 (38.6 mi^2) encompassing both the crest and flanks of the anticlinal trap, and is termed here as Distributed Crestal Leakage. The present-day gas-water contact is 85 m (278 ft), and the spill point is 110 m (328 ft) below the crest, implying that the trap is underfilled at present. The leakage zone comprises over 500 pockmarks at the present-day seabed with no crosscutting or cannibalization, suggesting that they formed in a short interval of time. These are underlain by sediment remobilization features and amplitude anomalies, consistent with a relatively high flux leakage of gas from the underlying Cretaceous deep-water sand-rich reservoir. By analyzing the geometrical relationship between the leakage zone, the top seal properties, and the gas-water contact, we conclude that the mode of leakage in this specific setting is not the result of gradual addition of gas charge but is instead consistent with a sudden increase of aquifer overpressure. We suggest two alternative models for seal failure in this case study: a conservative model consistent with a modest but rapid increase in aquifer overpressure leading to membrane seal failure, and a model dominated by high aquifer overpressure leading to leakage through hydraulically dilated faults and fractures.

INTRODUCTION

Leakage from top seals is a major cause of failure in exploration, resulting in underfilled or completely blown traps and in many sub-commercial discoveries (Downey, 1984; Rudolph and Goulding, 2017). Top seal failure leading to significant leakage is also a major risk for carbon sequestration in shallow saline aquifers (Chadwick et al., 2008), and is a particular point of focus for regulators (Bruant et al., 2002). A comprehensive understanding of the causes of top seal failure underpins all efforts to mitigate these risks, but with limited predictive capability to date and an estimated 50% of dry holes being attributable to some form of trap and seal failure (Rudolph and Goulding, 2017).

The theoretical foundations for top seal risking were established in a series of seminal papers published in the 1970s and 80s (Berg, 1975; Schowalter, 1979; Du Rouchet, 1981; Downey, 1984; England et al., 1987; Watts, 1987; Sales, 1997). These pioneering contributions emphasized the role of buoyancy pressure in determining seal capacity, whereby the maximum buoyancy pressure of a trapped hydrocarbon column (gas or oil or both) would be exerted on the base of the top seal at the position of the maximum hydrocarbon column (MHC; Figure 1A). For membrane seal failure (Schowalter, 1979), the failure would occur where the buoyancy force exceeded the capillary entry pressure of the top seal. For a homogeneous top seal with laterally uniform capillary properties, membrane leakage would occur at the position of MHC, which would typically be at the crestal point or close to that position (Figure 1A; Sales, 1997). Similarly, the likeliest point of failure of a seal through a mechanical or hydraulic seal failure mechanism (Watts, 1987) would also be at the MHC position, where the buoyancy pressure exceeds the minimum horizontal stress plus the tensile strength (Ingram and Urai, 1999). Hydrodynamic conditions in the aquifer would affect the column height required to achieve the match with either membrane or hydraulic seal failure conditions, and overpressured aquifers would be predicted to support smaller hydrocarbon columns than hydrostatically pressured aquifers (Schowalter, 1979; Heum, 1996).

Many traps are underfilled relative to the ultimate trap capacity defined by their spill points and this points to a limiting factor related either to hydrocarbon charge, or to leakage from top or lateral seals (Rudolph and Goulding, 2017). For a trap undergoing continuous charge, the trap would continue to fill

61 up to the spill point or until top seal failure and leakage occurred (Schowalter, 1979; Watts, 1987; Sales,
62 1997). Where top seal failure occurs before fill to spill, then it can be inferred that a critical column height
63 was reached (Class 2 and 3 traps, c.f. Sales, 1997), whereby any additional charge would increase the
64 column height such that the maximum buoyancy pressure exceeded either the membrane or the hydraulic
65 seal capacity (Figure 1B). Once the column height exceeds the seal capacity, any additional charge is
66 valved off through the leakiest portion of the top seal, resulting in a periodic, small scale discharge from
67 the weakest point in the seal, typically located directly above or close to the MHC position (Figure 1B)
68 (Showalter, 1979; Heum, 1996; Sales, 1997). So for leakage that is essentially the result of addition of
69 hydrocarbon charge into an underfilled trap, a highly focused leakage geometry would be the predicted
70 result, with the likeliest focus for the leakage being close to the position of the MHC. Deviations from
71 this expected geometry have been noted in cases where there are thief zones (high permeability layers
72 within the seal) or permeable faults that intersect the top reservoir downflank from the MCH position
73 (Hermanrud et al., 2014).
74 For traps receiving continuous, or semi-continuous charge, once the seal capacity is reached, a prolonged,
75 but low flux leakage would be expected as long as there is charge to increase the column height beyond
76 the seal failure threshold value (Sales, 1997) (Figure 1B). This type of leakage above hydrocarbon
77 accumulations worldwide in the form of gas chimneys or gas clouds is widely observed (Heggland, 1997;
78 Arntsen et al., 2007). The precise leakage geometry is often not possible to establish in these cases,
79 because of the poor imaging quality of reservoirs beneath gas chimneys on seismic data (Heggland,
80 1997). For ease of reference below, we refer to this mode of leakage as Localized Crestal Leakage, where
81 there is a single locus of leakage located close to or at the crest of the structure.
82 We present a case study of top seal leakage above a major gas field (the Scarborough Gas Field, NW
83 Shelf of Australia) where the seal bypass was evidently so efficient that just a minimum amount of
84 hydrocarbons were trapped in the seal and overburden, and no gas chimney developed as a result. This
85 means that the top seal and overburden are very well imaged above the field on a 3D seismic survey,
86 allowing us to map the seal bypass systems and seismic indicators for fluid flow and hence define the

leakage geometry (Cartwright et al. 2007). The seismic data shows that the leakage geometry contrasts markedly from that described above for localized crestal leakage, in that there are a number of leakage loci, rather than a single crestal focus, and that these occur over a large region (c. 100 km^2 [38.6 mi^2]) of the anticlinal trap, extending well down flank from the ultimate crestal position.

The near surface fluid expulsion features linked to the gas leakage strongly suggest that seal failure occurred in a geologically instantaneously manner in a single event. We discuss the failure conditions resulting in the leakage event, and that this type of distributed leakage geometry and geologically instantaneous timing of leakage cannot result from addition of gas charge. We then propose two models for seal failure in this setting: *Model A*, consistent with modest aquifer overpressure leading to membrane seal failure across top seal and overburden, and *Model B*, dominated by high aquifer overpressure leading to leakage through hydraulically opened faults and fractures. Both models are assessed and evaluated in relation to seal properties and the leakage mechanism that are require to justify the emplacement of the leakage phenomena observed above the Scarborough Gas Field.

SEISMIC AND WELL DATA

This study is based on a combination of high-resolution multichannel 2D seismic profiles, a 3D seismic volume, and well-log data from the NW Shelf of Australia (Figure 2). The 2D seismic grid AR NWS Regional and the HEX03A Scarborough 3D MSS three-dimensional seismic volume were released by the National Offshore Petroleum Titles Administrator (NOPTA) and made available for academic research purposes along with well data and selected well reports. The seismic cube, which is the key seismic data of this study, was acquired and processed by Western Geco in 2004. The acquisition was carried out using WesternGeco's Sleeveguns and 10 streamers spaced 75 m (246 ft) and with 320 group hydrophones each. The data was processed using a standard sequence for marine data and finalized to zero-phase European polarity convention (increase of acoustic impedance with depth is represented by a negative amplitude response; negative reflection coefficient = peak). The data is characterized by a vertical resolution of 7-10

112 m (22-32 ft) in the reservoir interval and shallower (Widess, 1973). The in-line and x-line spacing are
113 12.5 m (41 ft) and 18.75 m (61 ft), respectively.

114 The seismic volume HEX03A Scarborough 3D MSS was depth converted using 924 velocity functions
115 provided by NOPTA. The velocity functions were firstly smoothed with an operator of 300 ms in length,
116 and secondly combined to get an interval velocity field for the calculation of the time to depth conversion.
117 A QC of the individual functions was not possible because common mid points and relative semblance
118 displays were not available.

119 The creation of the velocity field and the time to depth conversion were completed using Hampson-
120 Russel software. The interpretation of the leakage phenomena, analyzed on the time volume, and the
121 horizons, produced by gridding of horizons picked on the depth-converted volume, were completed using
122 Schlumberger's Petrel software.

123

124 ## THE SCARBOROUGH GAS FIELD

125 ### Geological Context

126 The Scarborough Gas Field is located in the Exmouth Plateau, Carnarvon Basin (Figures 2A). The basinal
127 context is that of a rifted passive margin (the NW Shelf region) that now constitutes one of the major
128 hydrocarbon producing regions in Australia, with >130 trillion cubic feet of known reserves (Longley et
129 al., 2001; Drenth, 2007).
130 The basin experienced a number of rift phases in the Triassic, Late Jurassic, and Early Cretaceous,
131 expressed as an extensive array of large normal faults (Figure 2B-D). Clastic reservoirs were sourced
132 from the hinterland and transported to the basin to the northwest. The most widely exploited play in the
133 basin is based on reservoirs of Triassic age, such as the non-marine Mungaroo-Locker Formation (Boyd
134 et al. 1992). The Scarborough Field is reservoired in turbiditic sandstones of the Barrow Group (Early
135 Cretaceous) (Unit 1; Figure 2B). The immediately overlying Muderong Shale (Unit 2; Figure 2B-C) is a
136 deep marine hemipelagite deposited during the Mid Cretaceous and is the immediate top seal in the

Scarborough Field. Unit 2 is transected by a laterally extensive polygonal fault system (Cartwright, 2011), consisting of closely spaced normal faults with throws of a few tens of meters (Alrafee et al. 2018). Unit 3 was succeeded during the Late Cretaceous and Early Cenozoic by mainly pelagic carbonate mudstones (Unit 3; Figure 2B-C). A polygonal fault system, but a younger tier than that affecting Unit 2 also transects Unit 3, with little evidence of cross-tier propagation (Alrefaee et al. 2018; Figure 2C-D). The faults in Unit 2 and 3 exhibit a classical polygonal pattern with no evidence of any anisotropic horizontal stresses during their propagation (Figure 3A-B). The many faults in Unit 3 all tip out upwards at or very close to a prominent regional unconformity (Middle Miocene Unconformity; H1, Figures 2B-D, 3C) that formed during a major compressional event during the mid-late Miocene (Hillis et al., 2008). The unconformity was sculpted by erosion in a deep-water setting under the influence of strong bottom currents (Nugraha et al., 2018).

Tectonic compression led to the formation of NE-SW oriented structures across the basin, including the anticline hosting the Scarborough Gas Field (Jablonski et al., 2013). This compressional phase resulted in minor reactivation of tectonic normal faults and other inversion structures, such as minor parasitic folds (Figure 2C-D). There is no evidence of any reactivation of the polygonal faults in either Unit 2 or 3 during this phase of deformation (Figure 3C, 4A-B). The compression waned and died in the Late Miocene. Mid to late Miocene sediments (lowermost Unit 4; Figure 2B-3) onlap the flank of the Scarborough anticline suggesting that growth of this fold gradually died out during this interval (Figure 4A-C). This was followed by the pelagic drape of dominantly fine-grained carbonate successions (Unit 4; Figure 2B, 4A-C). No evidence of tectonic activity is evident at the present day in the NW Shelf region or above the Scarborough Field, although the maximum horizontal stress based on borehole breakouts and drilling-induced tensile fractures, is oriented perpendicular to the Miocene-aged fold axes (~113°N, Bailey et al., 2016).

Trap, seal and reservoir properties

The Scarborough Field was discovered in 1979, and subsequently five more wells and the 3D volume HEX03A Scarborough 3D were completed as a part of prolonged exploratory and appraisal campaigns under different operators. These well and data provided the information to characterize the properties and the geometries of the trap, the seal and the reservoir.

The trap of the Scarborough Gas Field is a four-way dip closure on an NNE elongated anticlinal dome (Figures 5A), with a modest relief of c. 110 m (328 ft) from crest to spill-point. The reservoir is offset by a number of NNE-SSSW and ENE-WSW trending normal faults (O'Halloran, 2006) with relatively modest throws of 10 to 20 m (32 to 65 ft) at top Reservoir (Figure 5B). These faults have much larger throws at the Triassic level, and their activity was quite limited within the Cretaceous (Bilal et al., 2018). They die out upwards in the middle of Unit 3 with no clear evidence of reactivation in this unit and in Unit 4 (Figure 2D).

The reservoir interval is composed of two main sand-rich basin-floor fans, namely the *Lower Fan* and the *Upper Fan*, with an average porosity of 20-30 % and a permeability of over 2000 mD. A prominent seismic flatspot (1) is mappable over the area of the field, (2) conforms to structure, and (3) matches the gas water contact (GWC) defined in the exploration and appraisal wells at 1916 m TVDSS (6286 ft; Figure 2B, 4A). The two reservoir units are in pressure communication as observed by the continuous and linear gas pressure gradients across these two sand rich formations (Figure 6A). Reserves of 7.3 trillion cubic feet of dry gas (95% methane, ~4% nitrogen) have been declared. The MHC is 84.7 m (278 ft; at well Scarborough-4; Locke, 2005). The water leg within the reservoir interval is hydrostatically pressured at the present day (Figure 6A). The trap is underfilled, with c. 35 m (c. 114 ft) of vertical separation between the actual gas-water contact and the spill-point.

The immediate top seal for the Scarborough Field is represented by the Muderong Formation (Unit 2, Figure 2B). In the field area, this is composed of c. 200 m (656 ft) of relatively homogeneous claystones with minor intercalations of limestone and silt (Figure 6B). The permeability of the Muderong Formation has been measured as 300 nD (Chen et al., 2014). The log signature is similarly uniform, with high gamma values throughout the interval (Figure 6B). Unit 2 is pervasively deformed by a polygonal fault

system (Alrafaee et al. 2018). There is no preferred orientation to these faults, as already observed in Figure 3A, and their spacing is a few hundred meters. Their maximum throws are typically less than 20 m (65 ft), and they die out at the Top Reservoir without offsetting this boundary (Figure 4A).

Leak-off test (LOT) results derived from the wells Scarborough-1 to 5 are plotted on a Pressure–Depth plot for the Scarborough Field along with mud weight data and fluid pressures within the water and gas legs (Figure 6A). The fracture gradient within the Muderong Formation is represented as a corridor to reflect the uncertainty in the LOT results and their distribution. The fracture gradient plotted in Figure 7 is a good match with the plot of minimum horizontal stress obtained from LOTs and Formation Integrity Tests from a larger well compilation of the Muderong Formation in the nearby Carnarvon Basin (Dewhurst and Hennig, 2003; Figure 7, inset). Simple construction assuming a constant gas gradient, as derived from the wells in the field, shows that the Muderong Formation seal has a hydraulic seal capacity (Watts et al., 1987) of between 530 and 760 m (1738 and 2493 ft) for gas (Figure 7). Because of the large number of faults and fractures a lower seal capacity is expected. Using the maximum mud weight profile (Scarborough-1) as representative of the most conservative value for seal capacity, a maximum gas column of 368 m (1207 ft) is obtained (Figure 7).

The membrane seal capacity is uncalibrated for the Muderong Formation in the Scarborough Gas Field, so we rely instead on a suite of measurements taken from exploration wells drilled about 200 km (124 mi) SE of the study area. Dewhurst et al. (2002) analyzed a 4 m (13 ft) long cored section taken directly above the reservoir in the lowermost Muderong Formation at 1120 m (3674 ft) below the seafloor. They computed values using a variety of methods and they obtained a mean value of 262 m (SD = 15.05) (860 ft) of equivalent gas column height for the local reservoir pressure and temperature conditions. In a later study, Kovack et al. (2004) extended these measurements to include mercury injection capillary pressure and compositional data from 24 wells over a large region of the Carnarvon Basin, located some 200 km (124 mi) SE of our study area. They found that the Muderong Formation exhibits a wide range of threshold pressure from 40 to 10,000 psi. Using the same database compiled by Kovack et al. (2004), but restricting the measurements to seven wells where the Muderong Formation is encountered at the same

depth range as in our study area, a mean value of threshold pressure of 1725 psi (SD = 716) was observed (11 MPa). The average gas column height of this subset of data in Kovack et al. (2004) calculated using in situ conditions, is 171 m (SD = 75) (561 ft) and equivalent to ~1.5 MPa (Figure 7). Both the locally derived hydraulic seal capacity (Figure 7) and the membrane seal capacity taken from Dewhurst et al. (2002) and Kovack et al. (2004) exceed the trap capacity.

A pronounced leakage zone has previously been recognized in the overburden and at the seabed in the south-central part of the field (Cowley and O'Brien, 2000; Jablonski et al. 2013) but no detailed analysis of geometry, timing or mechanism of leakage has been undertaken in previous studies.

LEAKAGE ZONE

The leakage zone was defined in our study by interpreting features indicative of gas migration through the units overlying the top reservoir, and up to the present-day seabed. These are described below in a top-down order on the HEX03A Scarborough 3D MSS time volume.

Seabed

The seabed exhibits smooth morphology and no signs of active erosion or disruption over most of the survey area (Figure 2D). The near surface sediments are not age calibrated in this area (no public domain data are available), but correlation using 2D seismic profiles to ODP 763, suggests that the first tens of meters could be Middle to Late Quaternary in age. This smooth seabed morphology is characteristic of the slow pelagic deposition in the area, but remarkably it is punctuated by a large sub-circular region of highly irregular seabed topography centered above the south-central part of the field (Figure 8A). A total of 522 small seabed depressions are mapped in the 3D seismic survey within an area of c.100 km^2 (38.6 mi^2). The depressions are demonstrably erosional (original sediments have been blown out by gas expulsion; Figure 8A-B), exhibit closed perimeters, with circular to sub-circular planforms and occur in a series of regions with high spatial density (Figure 8A). They typically measure 250-350 m (820-1050 ft)

across and their erosional relief at the seabed ranges from 10-25 m (32-82 ft). These depressions are interpreted as seabed pockmarks, based on their erosional character, planform, distribution and context (c.f. Judd and Hovland, 2009).

Unit 4

Unit 4 is bounded at its top by the seabed and at its base by the Middle Miocene Unconformity, shown as Horizon H1 in Figure 8B. Regionally, it is characterized by a parallel, laterally continuous seismic facies with weak amplitude reflections (Figure 2D, 4A). However, directly beneath the seabed pockmarks, this reflection character changes markedly, to a more discontinuous, or even chaotic seismic facies, with strong local amplification of small reflection sediments (Figure 8B). Vertically stacked concave-upwards reflections are commonly observed directly beneath the seabed pockmarks (Figure 8B).

These seismic characteristics collectively resemble zones of sediment disruption and remobilization formed due to focused fluid expulsion and gas migration (Judd and Hovland, 2009; Moss and Cartwright, 2010; Plaza-Faverola et al., 2011; Andresen and Huuse, 2011). Given that the only region with this disrupted seismic character occurs directly beneath the pockmarks, we interpret this seismic character to be the product of widespread fluid expulsion spanning the full region of the disrupted zone. There are seismic artifacts (transmission, attenuation) complicating the imaging of this disrupted volume, but these are interpreted to contribute to the seismic disruption rather than be its exclusive cause.

Middle Miocene Unconformity (Horizon H1)

A number of strong amplitude anomalies are mapped at and just below the unconformity precisely in the region below the pockmarks. Elsewhere, the unconformity is marked by a low to moderate amplitude reflection. These amplitude anomalies are acoustically hard (positive acoustic impedance contrast), and exhibit irregular planforms. These variably coalesce laterally where elongate portions follow the intersection of the unconformity with the upper tip portions of polygonal faults developed within Unit 3 (Figure 4A-B, 8C). These amplitude anomalies are similar in size and acoustic character to hydrocarbon-

265 related diagenetic zones that have been interpreted above many leaky hydrocarbon fields in the NW Shelf
266 petroleum province (Cowley and O'Brien, 2000). They are also very similar in geometry and acoustic
267 character to methanogenic carbonate cemented layers within vertical gas migration zones (Ho et al. 2012).
268 Although attenuation is observed beneath these anomalies, as would be expected, there are no obvious
269 velocity pull-ups or push-downs directly beneath. This could be taken to indicate that any cemented zones
270 or diagenetically altered layers were too thin for a noticeable velocity effect.
271
272 **Unit 3**
273 This seismic stratigraphic unit (Trella/Giralia Limestone, Miria/Korojon/Toolonga Formation, and Gearle
274 Siltstone, Figure 2B) is characterized regionally throughout the survey area by low to high amplitude
275 reflections with laterally continuous acoustic expression (Figure 4A). Their continuity is, however,
276 disrupted by closely spaced polygonal faults that transect this interval (Figure 3B, 4A, 8D-E). A number
277 of amplitude anomalies are observed within Unit 3 (Figure 8D-E-F). These are distributed near the top of
278 Unit 3, where they consist of vertically stacked reflections marked by soft and hard reflection pairs
279 (Figure 8D), and near the base of the same unit, where they occur more as isolated soft anomalies (Figure
280 8E). Both stacked and isolated anomalies have rounded planform shape as observed on map view (Figure
281 8F). The anomalies in Unit 3 do not produce signal deterioration i.e. their hosting stratigraphy is well
282 imaged within and around the amplification (Figure 8D-E). Because of the dominant soft polarity and the
283 fact that these anomalies are only observed in a small region above the underlying gas-water contact of
284 the Scarborough Gas Field, we interpret these features as gas-related amplitude anomalies. The stacked
285 anomalies near the top of Unit 3 are therefore interpreted as vertical anomaly clusters (VACs, Foschi et
286 al., 2014).
287
288 **Unit 2**
289 This unit is the immediate top seal to the reservoir for the Scarborough Field (Muderong Formation,
290 Figure 2B), and comprises generally low amplitude reflections whose lateral continuity is disrupted by a

lower tier of polygonal faults (Figure 3A, 4A). This is separated from the upper tier by a thin interval calibrated as the Windalia Radiolarite (H2, Figure 2B-C-D; Alexander et al., 1981). The only larger throw faults that transect this thin interval are the WNW-ESE and NNE-SSW trending tectonic normal faults that offset the top reservoir (Figure 3A, 5B). Small 100-meter's scale (328 ft) amplitude anomalies are observed in the upper section of this interval (Figure 8G-H). These are characterized by a dominantly soft polarity with amplitude above the background level (Figure 8G). On map view they are characterized by closely spaced 10-meter's scale anomalies separated at the intersection with the polygonal faults (Figure 8H). Because of the similarity with the other anomalies observed in Unit 3 we interpret these observed in Unit 2 as minor gas accumulations probably trapped within relatively higher porous intervals embedded within the Muderong Formation (e.g. Figure 6B, Scarborough-1, SWS #53, #52, #132).

Interpretation

Collectively, the fluid escape features at the seabed, and the seismic amplifications are all consistent with dominantly vertical gas migration, albeit with minor components of lateral migration as part of the generally upwards tortuous pathways (Figure 9A-B). Since the area affected by these phenomena forms a well-defined region exclusively above and within the gas-water contact of the Scarborough Field, we agree with previous interpretations that this suite of seismic features represents a large leakage zone above the field (O'Brien and Woods, 1995; Cowley and O'Brien, 2000; Jablonski et al., 2013).

The vertically stacked amplitude anomalies argue strongly for dominantly sub-vertical to vertical, probably tortuous, gas migration pathways whose loci are at the center of these anomaly stacks (c.f. Foschi et al., 2018). This points to the presence of a large number of localized vertical fluid migration pathways within the shallowest overburden units (Units 3 and 4) (Figure 9). This is also strongly suggested by the distribution of pockmarks into five sub-areas (Figure 8A, 9A). The spacing of these pockmarks and the structure of the seal units in the regions between the areas argues against an alternative interpretation that all of the widely dispersed near surface leakage phenomena could be linked to any

single leakage valve position. This is further emphasized by the presence of multiple, small scale gas pockets within the seal (Unit 2, Figure 8H), whose formation requires necessarily multiple loci and sub-vertical migration pathways.

The most surprising feature of this leakage zone is the lack of large gas-related seismic anomalies within Unit 2. This contrasts with many other leaky gas fields that typically have well defined gas chimneys embedded within the overburden (e.g. Tommeliten Alpha; Arntsen et al., 2007). Instead, above Scarborough, the evidence for leakage is almost entirely within the shallower units (3 and 4) rather than the immediate top seal (Unit 2). There are two possible contributory factors for this. Firstly, the polygonal faults may have acted as a highly efficient seal bypass system (Cartwright et al. 2007; Gay et al. 2007; Seebeck et al., 2015) (Figure 9B), preventing any significant local storage of gas en-route. Secondly, the dominantly claystone lithofacies of the Muderong Formation (Figures 2B, 6B) simply did not facilitate the significant storage of gas during its passage upwards.

DISCUSSION

The complex leakage phenomena observed above the Scarborough Gas Field encompasses a region of the top seal and overburden that extends vertically for over 700 m (2296 ft) and laterally for over 100 km^2 (38.6 mi^2; Figure 5B, 8A, 9A). Within this region of leakage, it is argued that there are a number of dominantly vertical migration foci, resulting in the formation of pockmarks at the seabed. When viewed in its entirety therefore, the leakage zone is a combined top seal and overburden volume that hosts a complex plumbing system connecting the top reservoir to the seabed (Figure 9B).

The sub-vertical components of the plumbing allowing cross-stratal gas migration and seal bypass are most likely the pre-existing polygonal faults (Figure 3), together with the smaller number of WNW and NNE trending tectonic normal faults (Figure 5A-B). In addition, some vertical flow paths may have been located coincident with the vertically stacked concave amplitude anomalies (Figure 8B, c.f. Foschi et al., 2018).

Importantly, this wide distribution of and large spacing between the vertical foci within the leakage zone argues that leakage could not be formed by a single valve point from the top reservoir, but instead argues positively for the presence of a series of more widely distributed points of leakage over a broad region of the crest of the trap (Figure 9B), which we term here Distributed Crestal Leakage. The distributed crestal leakage covers a broad region of the underlying Scarborough Gas Field, but does not extend beyond the lateral margin of the current GWC. Importantly, the distributed crestal leakage extends over a large portion of the broader crestal part of the field, where there is up to 40 m (131 ft) of relief at the top reservoir map (Figure 9A). This implies that the shallowest and deepest leakage loci would have been positioned above gas columns differing in height by 40 m (131 ft) at the time of leakage.

Timing of the leakage

When did this distributed leakage occur? The timing of the leakage can be constrained from the observation that there are present day seabed pockmarks. Hence the timing of the leakage 'event' is sufficiently recent to have left a clear morphological expression of seafloor pockmarks over a broad area, with no infilling or removal by erosion (Figure 8A). The absence of stacked pockmarks in the near surface sediments (c.f. Andresen and Huuse, 2011) argues in favor of a single, well defined leakage 'event' rather than an episodic series of leakage events. The duration of the event was sufficiently short so that no sign of cannibalization of adjacent pockmarks is seen in the seabed mapping (Figure 8B).

The timing of pockmark formation must post-date the youngest sediments that were eroded during pockmark formation. The pockmarks form at the seabed, but given the limits of vertical seismic resolution, it is not possible to differentiate pockmarks that formed recently with no subsequent sediment fill, from those that formed some time ago that have subsequently experienced a drape depositional infill (c.f. Moss et al. 2012). Modern deposition in this part of the passive margin is pelagic and sedimentation rates are low (c. 20 m/Ma [65 ft/Ma]), but the pristine geometry of the pockmarks imaged by the 3D seismic argues that the maximum thickness of any possible drape of younger pelagic sediment would be c. 5 m (16 ft; vertical resolution of the near seabed sediments). Nearby scientific boreholes (ODP sites

762 and 763) show that near surface sediments can be assigned to the Middle to Late Quaternary in age (Zone NN21b; Bolli et al. 1985). Hence, the leakage above the Scarborough Gas Field is interpreted to have occurred at some time (duration unknown) within the last 250 Ka.

Mechanisms of seal failure

The mechanism of seal failure is assessed in this section based on the geometry of the trap, the sealing properties of the immediate topseal (Muderong Formation), the geometry and seismic expression of the leakage zone, and the potential and the present day MHC observed at the Scarborough Gas Field.

The two widely accepted general mechanisms for topseal failure are membrane and hydraulic leakage (Watts, 1987). Since the membrane seal capacity for the Muderong Formation is uncalibrated in the study area, we must extrapolate from the nearest studies which are based on core and mercury injection capillary pressure data (Dewhurst et al., 2002; Kovack et al., 2004) and which indicate that a reasonable value for membrane seal capacity would be in the order of 170 – 260 m (561 – 853 ft; Figure 7). This disparity between seal capacity measurements and observed column heights has been attributed to leakage via critically stressed faults (Dewhurst and Hennig, 2003).

In contrast to the uncertainties in evaluating membrane seal capacity, the local calibration of the hydraulic seal capacity of the Muderong Formation for the Scarborough Field (Figure 7) suggests a much higher potential for retention of columns of at least 368 m (1207 ft), much greater than the trap capacity of 110 m (360 ft). Comparing the two types of seal capacity, and notwithstanding the uncertainties, it thus seems much more likely that the leakage event occurred by a process of membrane seal failure because the observed present day retained column height has a maximum value of 85 m (278 ft), much closer to the regional values of membrane seal capacity than the local hydraulic seal capacity. However, one additional uncertainty that should be borne in mind are the in situ stress conditions during the period of leakage, and whether these were likely to have led to critical stressing of any of the faults crossing the main seal units (Dewhurst and Hennig, 2003).

392 Based on the available seal property values, we suggest two alternative models, “Model A” and “Model
393 B” (Figure 10), for the leakage event above the Scarborough Field and conclude the discussion with an
394 assessment of their relative merits.
395
396 *“Model A”: Membrane Seal Failure*
397 We do not know if there is any leakage at present from the top of the reservoir, but there are no reported
398 indications of active leakage in the study area. We, therefore, assume that the 85 m (278 ft) MHC value is
399 an effective maximum seal capacity value for the Scarborough Gas Field at the present day. This effective
400 seal capacity would include the contributions of polygonal faults and fractures above the region with the
401 MHC. Because there are no obvious changes in the spacing, throw value or orientation of the polygonal
402 fault system across the structure (Figure 3), there is no obvious reason to invoke a lateral variation in
403 effective seal capacity, such that the regions down flank would most likely have a similar seal capacity.
404 Based on this, we suggest that a minimum leakage criterion for the downflank areas, with present day
405 column heights of c. 40 m (131 ft), would have been a value equivalent to the present day MCH, i.e. 85 m
406 (278 ft). This then implies that a minimum additional gas pressure of 0.35 MPa, equivalent to a column of
407 ~45 m (147 ft) of gas at identical reservoir P-T conditions would have been required to produce failure of
408 the topseal in the downflank regions. Such an additional pressure source could have arisen from a modest
409 increase in aquifer pressure, of 0.35 MPa above the current hydrostatic condition, but we suggest that this
410 increase would need to have been relatively rapid in order to lead to synchronous leakage from both
411 crestal and downflank leakage loci (Figure 10). Alternatively, a surge in gas migration into the trap could
412 also have led to conditions favoring distributed leakage, but this would also have had to have been rapid.
413 Slow increase in the hydrocarbon column height across the field would have led instead to localized
414 crestal leakage (Figure 1) (Sales, 1997).
415
416 *“Model B”: Hydraulic Seal Failure*

In contrast to the conservative conditions discussed above for "Model A", the reservoir/aquifer conditions for hydraulic seal failure are much more extreme. For purely hydraulic seal failure involving the polygonal fault network and perhaps additionally the E-W trending tectonic faults, the gas pressure would have needed to be greater than that equivalent to a >520 m (1706 ft) column height, to intersect the fracture gradient window, and 368 m (1207 ft) to reopen and reactivate preexisting faults and fractures (Figure 7). Since the spill point is only 110 m (360 ft) below the crest of the structure, such a large gas column could not have accumulated, so the only way to achieve the necessary pressure is with some combination of increased gas column and aquifer overpressuring. The aquifer overpressure required for a gas column of a completely filled-to-spill structure would have been of the order of 3.5 MPa, which again reduces to 2.1 MPa for preexisting faults and fractures (Figure 7). The build-up of this substantial overpressure would also have to have been rapid, as with "Model A", or crestal leakage would dominate and lead to pressure reduction before the full dimensions of the leakage zone could be established.

For failure of the topseal in shear mode, it is conceivable that much lower values of gas pressure could have induced shear failure of the pre-existing faults and fractures in the topseal, and in turn led to leakage from a number of fault-related loci. It is difficult to assess this possibility for the Scarborough Gas Field (see Underschultz and Strand, 2016 for theoretical considerations of pressure induced reactivation of critically stressed faults) because there are no cores calibrating the shear strength of the fractured Muderong Formation and in situ stress conditions are also uncalibrated. The fact that a polygonal fault system is pervasively developed within the seal and is clearly imaged by the seismic perhaps indicates the presence of a network of sub-seismic fractures too (Cartwright, 2011), and it is certainly a possibility that some subset of these fractures might have favorable orientations to be critically stressed in the present-day stress field. If so, then increases in gas pressure at the reservoir/seal interface could then have promoted leakage, as suggested by Dewhurst and Hennig (2003).

"Model A" versus "Model B"

Two key questions need to be addressed in assessing the relative merits of the two models proposed here. Firstly, would the specific leakage mechanism and pressure conditions lead to the observed leakage zone characteristics, and secondly, how does each model accord with the observed timing of surface leakage that formed the pockmark field?

For "Model A", the strength of the envisaged conservative pressure conditions is that it is much easier to envisage how a modest increase in aquifer pressure could be achieved, and following leakage, why the aquifer would then return to a background hydrostatic pressure, as currently observed. However, with such a low overpressure, it is difficult to conceive that flux of gas from the reservoir through the very low permeability Muderong Formation (300 nD) would be high enough after c. 900 m (2952 ft) of vertical ascent to lead to pockmark formation, sediment remobilization and seabed subsidence (Figure 8A, B and D). It is also hard to understand why, in a membrane leakage model, there is not more evidence of gas pockets trapped in the thin-bedded siltstones within the seal (Figure 6B) and overburden (e.g. Gearle Siltstone, Unit 3, Figure 2B), since these would have been important percolation flow pathways for gas migration through the generally fine-grained succession due to their orders of magnitude lower entry pressure values (e.g. Nelson, 2009).

One major uncertainty in the membrane leakage analysis is the specific role of the polygonal faults. At first inspection, these seem to offer the most obvious weak points for the seal, and since they are pervasive throughout the Muderong Formation and much of the overburden, they offer plausible pathways for leaking hydrocarbons. As argued above, they may lower the effective membrane seal capacity compared to values at the core scale, but they cannot by themselves explain the 40 m (131 ft) range in the top reservoir depth values and gas column values for the various leakage loci. To do so, we would have to explain why the polygonal faults at the crestal location differ from those down flank in their contribution to a two-fold apparent variation in effective seal capacity, when there is no seismically visible evidence for any lateral variation in their structural characteristics (Figures 3 and 4).

For "Model B", a hydraulic mechanism is appealing, it is much more likely to deliver large fluxes of gas through the fault and fracture networks by dilation under elevated pressure, since dilatant fractures would

allow open aperture channel flow conditions across almost the full thickness of the overburden, or at least to within 100 m (328 ft) or so of the seabed (Unit 4; Figures 4A and 8A). However, even with some element of critical stressing of a subset of the fracture population, the LOT data (Figure 7) imply a very significant and rapid increase in aquifer pressure as a fundamental requirement to drive this leakage mode. Although overpressured compartments of 20 MPa above hydrostatic have been documented in some region of the Northern Carnarvon Basin (e.g. He et al., 2002, 200 km to the SE of the study area) there is no evidence in our study area to account for such a dramatic pressure increase. We cannot exclude this Model as such, but the lack of a viable mechanism to explain even the conservative 2.1 MPa aquifer pressure increase is a significant deficiency of this model at present.

On balance therefore, although neither model is without its weaknesses, we favor "Model A", and a conservative view of the leakage mechanism as being dominated by membrane leakage processes.

Implications

The flux during the leakage event is unknown, but from the scale and mechanism of leakage proposed, we suggest that it must have been sufficient to exploit the enhanced permeability derived from pre-existing faults and form the large pockmark field observed at the seabed. However dramatic the scale of the leakage zone is, it is nevertheless hazardous to view the volume of the leakage zone as a proxy for total leaked hydrocarbon volumes. In the example we present here, it is likely that most of the leaked gas bypassed most of the seal and overburden and that only a small fraction of the total leaked methane remains trapped in the subsurface, as evidenced by the presence of shallow amplitude anomalies. In other examples of leaky gas fields, the evidence for leakage is often expressed seismically as a gas chimney, where large rock volumes within the chimney feature may contain only low saturation gas, distributed in relatively small pockets (e.g. Arntsen et al. 2007). Much further work is therefore required before leakage events like the one described here from Scarborough can be fully quantified.

CONCLUSIONS

The main conclusions are as follows:

1. The Scarborough Gas Field, a 7.3 trillion cubic feet hydrocarbon accumulation located in the NW Shelf of Australia, experienced a major seal failure in the past 250 Ka.
2. The seal failure produced a 100 km^2 (38 mi^2) wide leakage zone composed of over 500 pockmarks and sediment remobilization at the seabed and stacked shallow gas accumulations in the overburden.
3. The geometry of the leakage zone is consistent with multiple points of seal failure from where the gas escaped from the reservoir to the water column bypassing efficiently the seal and the overburden.
4. The most likely cause of seal failure is by a rapid increase in aquifer pressure by a minimum value of c. 0.35 MPa. This would account for the c.40 m (131 ft) variation in the column heights presently found beneath the widely distributed leakage foci.

REFERENCES

Alexander, R., Kagi, R.I. and Woodhouse, G.W., 1981. Geochemical correlation of Windalia oil and extracts of Winning Group (Cretaceous) potential source rocks, Barrow Subbasin, Western Australia. AAPG Bulletin, 65(2), pp.235-250.

Alrefaee, H. A., S. Ghosh, and M. I. Abdel-Fattah, 2018, 3D seismic characterization of the polygonal fault systems and its impact on fluid flow migration: An example from the Northern Carnarvon Basin, Australia: Journal of Petroleum Science and Engineering, v. 167, pp. 120-130.

Andresen, K.J. and Huuse, M., 2011. 'Bulls-eye' pockmarks and polygonal faulting in the Lower Congo Basin: relative timing and implications for fluid expulsion during shallow burial. Marine Geology, 279(1-4), pp.111-127.

Arntsen, B., Wensaas, L., Løseth, H. and Hermanrud, C., 2007. Seismic modelling of gas chimneys. Geophysics, 72(5), pp.SM251-SM259.

Bilal, A., McClay, K. and Scarselli, N., 2018. Fault-scarp degradation in the central Exmouth Plateau, North West Shelf, Australia. Geological Society, London, Special Publications, 476, pp.SP476-11.

Bailey, A.H., King, R.C., Holford, S.P. and Hand, M., 2016. Incompatible stress regimes from geological and geomechanical datasets: can they be reconciled? An example from the Carnarvon Basin, Western Australia. Tectonophysics, 683, pp.405-416.

Berg, R.R., 1975. Capillary pressures in stratigraphic traps. AAPG bulletin, 59(6), pp.939-956.

Boyd, R., Williamson, P. and Haq, B.U., 1992. Seismic stratigraphy and passive-margin evolution of the southern Exmouth Plateau. Sequence Stratigraphy and Facies Associations, pp.579-603.

Bolli H. M., Saunders J. B. & Perch-Nielsen K. (eds.) 1985. Plankton Stratigraphy. VIII, 1032 pp. Cambridge, London, New York, New Rochelle, Melbourne, Sydney: Cambridge University Press.

Bruant, R., Guswa, A., Celia, M. and Peters, C., 2002. Safe Storage of CO~ 2 in Deep Saline Aquifers. Environmental Science And Technology-Washington DC-, 36(11), pp.240A-245A.

Cartwright, J., 2011. Diagenetically induced shear failure of fine-grained sediments and the development of polygonal fault systems. Marine and Petroleum Geology, 28(9), pp.1593-1610.

Cartwright, J., Huuse, M. and Aplin, A., 2007. Seal bypass systems. AAPG bulletin, 91(8), pp.1141-1166.

Chadwick, A., Arts, R., Bernstone, C., May, F., Thibeau, S. and Zweigel, P., 2008. Best Practice for the Storage of CO2 in Saline Aquifers-Observations and Guidelines from the SACS and CO2STORE projects (Vol. 14). British Geological Survey.

Chen, Z., Zhou, F. and Rahman, S.S., 2014. Effect of cap rock thickness and permeability on geological storage of CO2: laboratory test and numerical simulation. Energy Exploration & Exploitation, 32(6), pp.943-964.

Cowley, R. and O'brien, G.W., 2000. Identification and interpretation of leaking hydrocarbons using seismic data: A comparative montage of examples from the major fields in Australia's northwest shelf and Gippsland basin. The APPEA Journal, 40(1), pp.119-150.

Dewhurst, D.N., Jones, R.M. and Raven, M.D., 2002. Microstructural and petrophysical characterization of Muderong Shale: application to top seal risking. Petroleum Geoscience, 8(4), pp.371-383.

Dewhurst, D.N. and Hennig, A.L., 2003. Geomechanical properties related to top seal leakage in the Carnarvon Basin, Northwest Shelf, Australia. Petroleum Geoscience, 9(3), pp.255-263.

Downey, M.W., 1984. Evaluating seals for hydrocarbon accumulations. AAPG bulletin, 68(11), pp.1752-1763.

Drenth, M., 2007. Petroleum and Minerals Industries in the Northwest Marine Region. International Risk Consultants Pty Limited, Report Number: ENV-REP-07-0086 Rev 0.

Du Rouchet, J., 1981. Stress fields, a key to oil migration. AAPG bulletin, 65(1), pp.74-85.

England, W.A., Mackenzie, A.S., Mann, D.M. and Quigley, T.M., 1987. The movement and entrapment of petroleum fluids in the subsurface. Journal of the Geological Society, 144(2), pp.327-347.

Foschi, M., Cartwright, J.A. and Peel, F.J., 2014. Vertical anomaly clusters: Evidence for vertical gas migration across multilayered sealing sequences. AAPG Bulletin, 98(9), pp.1859-1884.

Foschi, M., Cartwright, J.A. and MacMinn, C.W., 2018. Sequential vertical gas charge into multilayered sequences controlled by central conduits. AAPG Bulletin, 102(5), pp.855-883.

561 Gay, A., Lopez, M., Berndt, C. and Seranne, M., 2007. Geological controls on focused fluid flow
562 associated with seafloor seeps in the Lower Congo Basin. Marine Geology, 244(1-4), pp.68-92.

563 He, S., Middleton, M., Kaiko, A., Jiang, C. and Li, M., 2002. Two case studies of thermal maturity and
564 thermal modelling within the overpressured Jurassic rocks of the Barrow sub-basin, north west
565 shelf of Australia. Marine and Petroleum Geology, 19(2), pp.143-159.

566 Heggland, R., 1997. Detection of gas migration from a deep source by the use of exploration 3D seismic
567 data. Marine Geology, 137(1-2), pp.41-47.

568 Hermanrud, C., Halkjelsvik, M.E., Kristiansen, K., Bernal, A. and Strömbäck, A.C., 2014. Petroleum
569 column-height controls in the western Hammerfest Basin, Barents Sea. Petroleum Geoscience,
570 20(3), pp.227-240.

571 Heum, O.R., 1996. A fluid dynamic classification of hydrocarbon entrapment. Petroleum Geoscience,
572 2(2), pp.145-158.

573 Hillis, R.R., Sandiford, M., Reynolds, S.D. and Quigley, M.C., 2008. Present-day stresses, seismicity and
574 Neogene-to-Recent tectonics of Australia's 'passive'margins: intraplate deformation controlled by
575 plate boundary forces. Geological Society, London, Special Publications, 306(1), pp.71-90.

576 Ho, S., Cartwright, J.A. and Imbert, P., 2012. Vertical evolution of fluid venting structures in relation to
577 gas flux, in the Neogene-Quaternary of the Lower Congo Basin, Offshore Angola. Marine
578 Geology, 332, pp.40-55.

579 Ingram, G.M. and Urai, J.L., 1999. Top-seal leakage through faults and fractures: the role of mudrock
580 properties. Geological Society, London, Special Publications, 158(1), pp.125-135.

581 Jablonski, D., Preston, J., Westlake, S., Gumley, C.M., 2013. Unlocking the origin of hydrocarbons in the
582 central part of the Rankin Trend, Northern Carnarvon Basin, Australia. In: Keep, M., Moss, S.J.
583 (Eds.), The Sedimentary Basins of Western Australia IV: Proceedings of the Petroleum
584 Exploration Society of Australia Symposium Exploration Society of Australia, pp. 1–31.

585 Judd, A. and Hovland, M., 2009. Seabed fluid flow: the impact on geology, biology and the marine
586 environment. Cambridge University Press.

587 Kovack, G.E., Dewhurst, D.N., Raven, M.D. and Kaldi, J.G., 2004. The influence of composition,
588 diagenesis and compaction on seal capacity in the Muderong Shale, Carnarvon Basin. The
589 APPEA Journal, 44(1), pp.201-222.

590 Locke, 2005. WA-1-R Scarborough-3 & -3/CH1 Well Completion Report - Interpretive Volume. BHP
591 Billiton Petroleum PTY. LTD. A.B.N. 97 006 918 832.

592 Longley, I.M., Bradshaw, M.T. and Hebberger, J., 2001. AAPG Memoir 74, Chapter 15: Australian
593 petroleum provinces of the twenty-first century.

594 Moss, J.L. and Cartwright, J., 2010. 3D seismic expression of km-scale fluid escape pipes from offshore
595 Namibia. Basin Research, 22(4), pp.481-501.

596 Moss, J.L., Cartwright, J. and Moore, R., 2012. Evidence for fluid migration following pockmark
597 formation: Examples from the Nile Deep Sea Fan. Marine Geology, 303, pp.1-13.

598 Nelson, P.H., 2009. Pore-throat sizes in sandstones, tight sandstones, and shales. AAPG bulletin, 93(3),
599 pp.329-340.

Nugraha, H.D., Jackson, C.A., Johnson, H.D., Hodgson, D.M. and Reeve, M.T., 2019. Tectonic and oceanographic process interactions archived in Late Cretaceous to Present deep-marine stratigraphy on the Exmouth Plateau, offshore NW Australia. Basin Research, 31(3), pp.405-430.

O'Halloran, 2006. Scarborough HEX03A 3D Seismic Survey - Interpretation Report WA-1-R Exmouth Plateau, BHP Billiton Petroleum PTY. LTD. A.B.N. 97 006 918 832.

Plaza-Faverola, A., Bünz, S. and Mienert, J., 2011. Repeated fluid expulsion through sub-seabed chimneys offshore Norway in response to glacial cycles. Earth and Planetary Science Letters, 305(3-4), pp.297-308.

Rudolph, K.W. and Goulding, F.J., 2017. Benchmarking exploration predictions and performance using 20+ yr of drilling results: One company's experience. AAPG Bulletin, 101(2), pp.161-176.

Sales, J.K., 1997. AAPG Memoir 67: Seals, Traps, and the Petroleum System. Chapter 5: Seal Strength vs. Trap Closure--A Fundamental Control on the Distribution of Oil and Gas.

Schowalter, T.T., 1979. Mechanics of secondary hydrocarbon migration and entrapment. AAPG bulletin, 63(5), pp.723-760.

Seebeck, H., Tenthorey, E., Consoli, C. and Nicol, A., 2015. Polygonal faulting and seal integrity in the Bonaparte Basin, Australia. Marine and Petroleum Geology, 60, pp.120-135.

Underschultz, J. and Strand, J., 2016. Capillary seal capacity of faults under hydrodynamic conditions. Geofluids, 16(3), pp.464-475.

Watts, N.L., 1987. Theoretical aspects of cap-rock and fault seals for single-and two-phase hydrocarbon columns. Marine and Petroleum Geology, 4(4), pp.274-307.

Widess, M.B., 1973. How thin is a thin bed?. Geophysics, 38(6), pp.1176-1180.

Figure 1. A, cartoon and pressure-depth plot of a simplified gas accumulation hosted within a representative sand interval and trapped by a representative seal. At the base of the seal the gas exerts a pressure proportional to the maximum hydrocarbon column (MHC). The MHC is located at the shallowest point of the reservoir. The pressure exerted by the gas is insufficient to fracture the seal i.e. the gas gradient (GG) does not intersect the fracture gradient (FG); HG = hydrostatic gradient. B, the increase of the MHC (during gas charging) produces a higher gas pressure, which is sufficient to breach the seal and produce leakage. The leakage will occur at the MHC and within the nearby region (localised crestal leakage).

Figure 2. A, The Exmouth Plateau is located in the North West shelf of Australia (inset). The three-dimensional seismic data and two regional two-way time (TWT) profiles shown in this study are located along a NE-SW trending anticline within the Exmouth Plateau. ODP 763 provides information for the dating of the sediments near the seabed, which based on radiolarians collected at ODP Site 763 (c. tuberose and b. invaginata), are Middle to Late Quaternary in age (Bolli et al., 1985). B, representative stratigraphic column of the Exmouth Plateau (from Nicoll et al., 2009), with the main subdivision in units described in the text. Bold names refer to formations encountered by the exploration boreholes intersecting the 3D seismic volume. C, regional profile depicting the regional structural and stratigraphic features of the basin, with gross subdivision in 4 main units. D, regional profile intersecting the gas water contact (GWC) of the Scarborough Gas Field.

Figure 3. A, coherence attribute and depth structural maps of the base of the Muderong Formation intersected by the Triassic normal faults and the polygonal faults (refer to Figure 4A for the position). The polygonal faults are closely spaced and exhibit polygonal pattern without any significant evidence of preferential strike development. B, time-slice of a coherence attribute volume across the center of Unit 3 depicting the polygonal character of the polygonal faults (refer to Figure 4A for the position). The polygons do not show any evidence of preferential strike development. C, time-slice of a coherence attribute volume across the center of Unit 4 (refer to Figure 4A for the position). Unit 4 does not show any evidence of polygonal faults. At the center of the map a large disruption zone can be observed.

Figure 4. A, depth seismic cross section (see Figure 4 for line location) depicting the main structural elements of the Scarborough Gas Field and the leakage zone. The Scarborough Gas Field exhibits a gas water contact (GWC) at 1916 m (6286 ft). Horizon 3 (H3) represents the top of the reservoir of the combined Upper and Lower Fans. Unit 2 represents the sealing unit and Unit 3 and 4 the overburden. Unit 2 and 3 are offset by two independent polygonal fault systems (PFS). Amplitude anomalies (AAs) are observed at the top of Unit 3 (described later). At the seabed surface pockmarks (PM) affect the seabed morphology (described later). B, displacement versus depth profiles of five representative polygonal faults across Unit 2 (see Figure 4A for location). The maximum displacement is observed at around 300 m (984 ft) below the Middle Miocene Unconformity (H1, datum). The upper tip of the polygonal faults is truncated at H1 suggesting that the top was eroded during the formation of the unconformity. C, 2x close up (see Figure 4A for location) showing the onlapping geometry of Unit 4 on H1.

Figure 5. A, depth structural map of H3 (top reservoir of the combined Lower and Upper Fans) around the 3D seismic volume. The map was constructed using regional two-way-time profiles. The map was depth converted using an average interval velocity for the seal, the overburden and the water. The spill point (SP) of H3 is located in the NE corner of the map at a depth of 1960-1965 m (6430-6446 ft). B, depth structural map of H1 with structural elements, gas water contact (GWC) and position of the exploration borehole. The GWC is located at an average depth of 1900-1920 m (6233-6299 ft).

Figure 6. A, pressure-depth plot derived from data retrieved at the exploration boreholes Scarborough-1 to 5 (no data was available from well North Scarborough-1; pressure data at Scarborough-3 is offset because of a different gauge device). The data shows that the water gradient is in hydrostatic equilibrium at the well locations. The gas gradient is constant for all the wells suggesting good hydraulic communication within the reservoir. The gas water contact (GWC) can be observed at the intersection between the hydrostatic and the gas gradients at c. 1936 m (6351 ft) measured depth (MD; 1916 m [6286 ft] true vertical depth at sea surface, TVDSS). The top reservoir (top Upper Fan, Top UF). The fracture gradient was constructed using leak-off test (LOT) pressures collected at different depth intervals. A linear gradient was used. B, gamma ray versus depth cross plot from the exploration boreholes Scarborough-1 to 5 with lithological information derived from side-wall samples (SWS) and cuttings. The Muderong Formation is characterised by a variable thickness of 150 and 220 m (492 and 721 ft). It is characterised by large gamma ray readings and is dominated by claystone with a few intercalations of calcareous siltstone.

Figure 7. Pressure-depth plot derived from data retrieved at the exploration boreholes Scarborough-1 to 5 (no data was available from well North Scarborough-1; see Figure 6A for reference). The fracture gradient was constructed using leak-off test (LOT) pressures collected at different depth intervals. Using a linear interpolation a fracture pressure gradient of 16.3 MPa/km was obtained (this gradient is compared to what obtained by Dewhurst and Hennig, 2003, inset). Using the gas pressure gradient retrieved from the borehole Scarborough-1 to 5 a series of gas columns were plotted. The gas gradient exerted by the current gas column and up to the spill point is not sufficient to breach the seal. A hypothetical gas column of at least 526 m (1725 ft) is necessary to fracture the seal. A column of 368 m (1207 ft) would be required to reopen or reactivate pre-existing faults and fractures. The plot also shows the hypothetical gas columns required to capillary invade the seal (>171 m [561 ft]). These are estimated based on two works completed by Dewhurst et al., 2002 (Pce^1) and Kovack et al., 2004 (Pce^2) (see text).

Figure 8. Composite figure of the main leakage phenomena observed above the Scarborough Gas Field. A, seabed map showing the position of the 522 pockmarks (yellow dots) enclosed within five pockmark regions (R1 to R5, dashed blue line). The pockmark regions are defined using a density function calculated from the distribution of the pockmarks, where grey is low density and yellow is high density. B, seismic cross section depicting the shallow section of the study area (see Figure 8B for line location). Unit 4 exhibits concave upward reflections below the pockmarks interpreted as sediment remobilization and collapse produced by the migration of fluids. C, amplitude map showing the amplitude response of horizon H1 (Middle Miocene Unconformity; see figure 8A for map location). The root-mean square (RMS) amplitude response shows stellate anomalies distributed along the intersection of polygonal faults (PF) and H1 surface. These suggest a migration mechanism dominated by vertical migration along polygonal faults (see text). D, seismic cross section depicting a representative vertical anomaly cluster (VAC, see Figure 8C for line location). These VACs are characterized by a limited extent and are composed of 4-5 anomalies each. The polygonal fault system (PFS) may prevent significant lateral migration. E, seismic cross section depicting amplitude anomalies encountered in the lower section of Unit 3 (see Figure 8C for line location). F, amplitude extraction showing the shape of the amplitude anomalies (AA) in the lower section of Unit 3 and the polygonal faults (PF). G, seismic cross section showing the acoustic response of minor amplitude anomalies observed in Unit 2. These are a few tens of meters in size and are located just a few hundreds of meters above the top reservoir (H3). H, amplitude map showing the acoustic characteristic of the amplitude anomalies (AA) observed in Unit 2. These are grouped in small ensembles separated by polygonal faults (PF).

Figure 9. A, distribution of leakage phenomena observed above the Scarborough Gas Field (gas water contact, GWC, after Locke, 2005) and depth contour of the top reservoir (Horizon H3). There is a vertical stacking of the individual amplitude anomalies and pockmarks observed at the different units above the gas field. The leakage phenomena are located along the tectonic normal faults, above structural crests and along the flanks of the structural closure. Importantly, the leakage phenomena are located above gas columns of different heights. B, synoptic section showing the shallow plumbing system above the Scarborough Gas Field. The occurrence of deep and shallow anomalies and the pockmarks at the seabed, and the lack of signal deterioration, allows reconstructing the likely scenario for gas migration across the seal and the overburden (Unit 2 and 3). The polygonal faults seems playing a dominant role as seal bypass. The lack of prominent amplitude anomalies indicate the poor storage capacity of Unit 2 and 3. The occurrence of multiple amplitude anomalies near the top reservoir, and importantly within the seal (Unit 2), implies the presence of multiple valve points or loci from where the gas leaks across the seal and the overburden.

Figure 10. Simplified cartoons showing hypothetical scenarios of gas leakage above a gas field characterized by a maximum seal capacity equivalent to an 85 m (278 ft) gas column, and maximum trap capacity of ~110 m (360 ft). The seal and the overburden are both affected by polygonal faults. Model A: a rapid increase of gas column (up to the spill point), or aquifer pressure, results into a sudden overpressure of about 0.35 MPa. This overpressure is sufficient to produce a capillary failure at the crest and in the downflank regions of the seal where the gas column is 40 – 45 m (131 – 147 ft). The capillary leakage is characterized by a relatively weak gas flow across more permeable routes, such as the polygonal faults. Model B: a rapid increase of aquifer overpressure of 3.26 MPa dilates preexisting faults and fractures. The large hydrocarbon flow across the hydraulically opened faults produces a large leakage zone consisting of seabed pockmarks, sediment remobilization and seabed collapse.

733

FIGURE 1

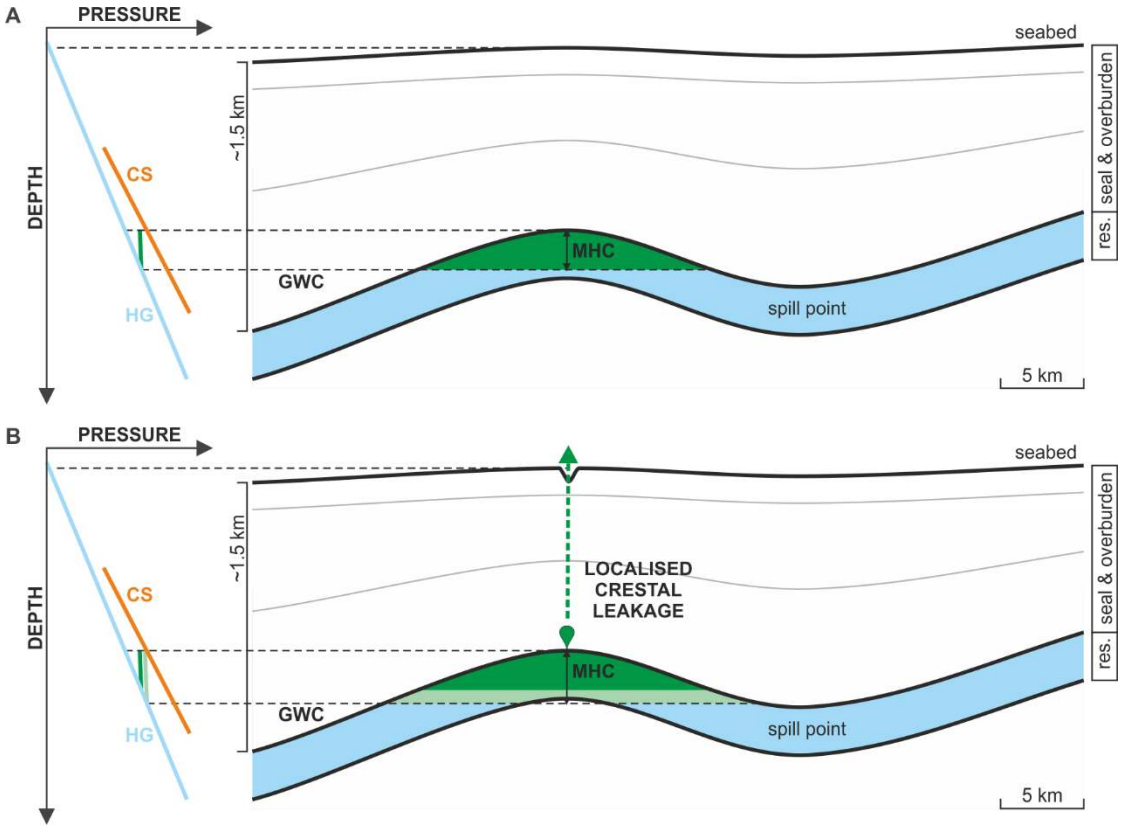
A
PRESSURE
DEPTH
CS
HG
~1.5 km
seabed
MHC
GWC
spill point
res.
seal & overburden
5 km
B
PRESSURE
DEPTH
CS
HG
~1.5 km
LOCALISED
CRESTAL
LEAKAGE
seabed
MHC
GWC
spill point
res.
seal & overburden
5 km

FIGURE 2

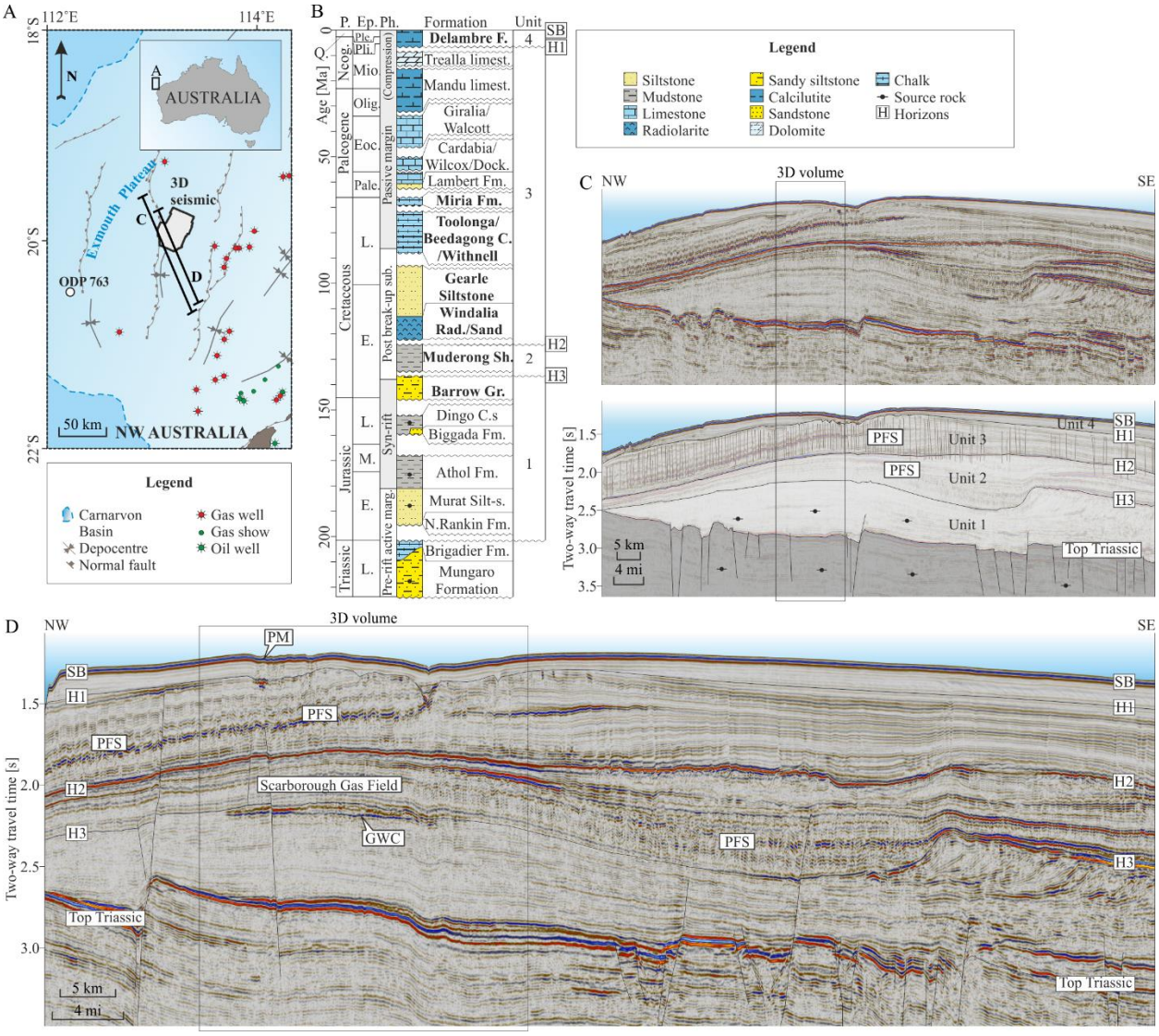
A
112°E
114°E
18°S
20°S
22°S
N
AUSTRALIA
3D seismic
C
D
Exmouth Plateau
ODP 763
50 km
NW AUSTRALIA
Legend
Carnarvon Basin
Depocentre
Normal fault
Gas well
Gas show
Oil well
B
P. Ep. Ph.
Formation
Unit
Age [Ma]
Q.
Neog.
Paleogene
Cretaceous
Jurassic
Triassic
Plio.
Pli.
Mio.
Olig.
Eoc.
Pale.
L.
E.
M.
Passive margin (Compression)
Post break-up sub.
Syn-rift
Pre-rift active marg.
Delambre F.
Trealla limest.
Mandu limest.
Giralia/ Walcott
Cardabia/ Wilcox/Dock.
Lambert Fm.
Miria Fm.
Toolonga/ Beedagong C. /Withnell
Gearle Siltstone
Windalia Rad./Sand
Muderong Sh.
Barrow Gr.
Dingo C.s
Biggada Fm.
Athol Fm.
Murat Silt-s.
N.Rankin Fm.
Brigadier Fm.
Mungaro Formation
SB
H1
H2
H3
Legend
Siltstone
Mudstone
Limestone
Radiolarite
Sandy siltstone
Calcilutite
Sandstone
Dolomite
Chalk
Source rock
Horizons
C
NW
SE
3D volume
PFS
Unit 4
Unit 3
Unit 2
Unit 1
Top Triassic
Two-way travel time [s]
5 km
4 mi
D
NW
SE
3D volume
PM
PFS
Scarborough Gas Field
GWC
Top Triassic
Two-way travel time [s]
5 km
4 mi

740 **FIGURE 3**

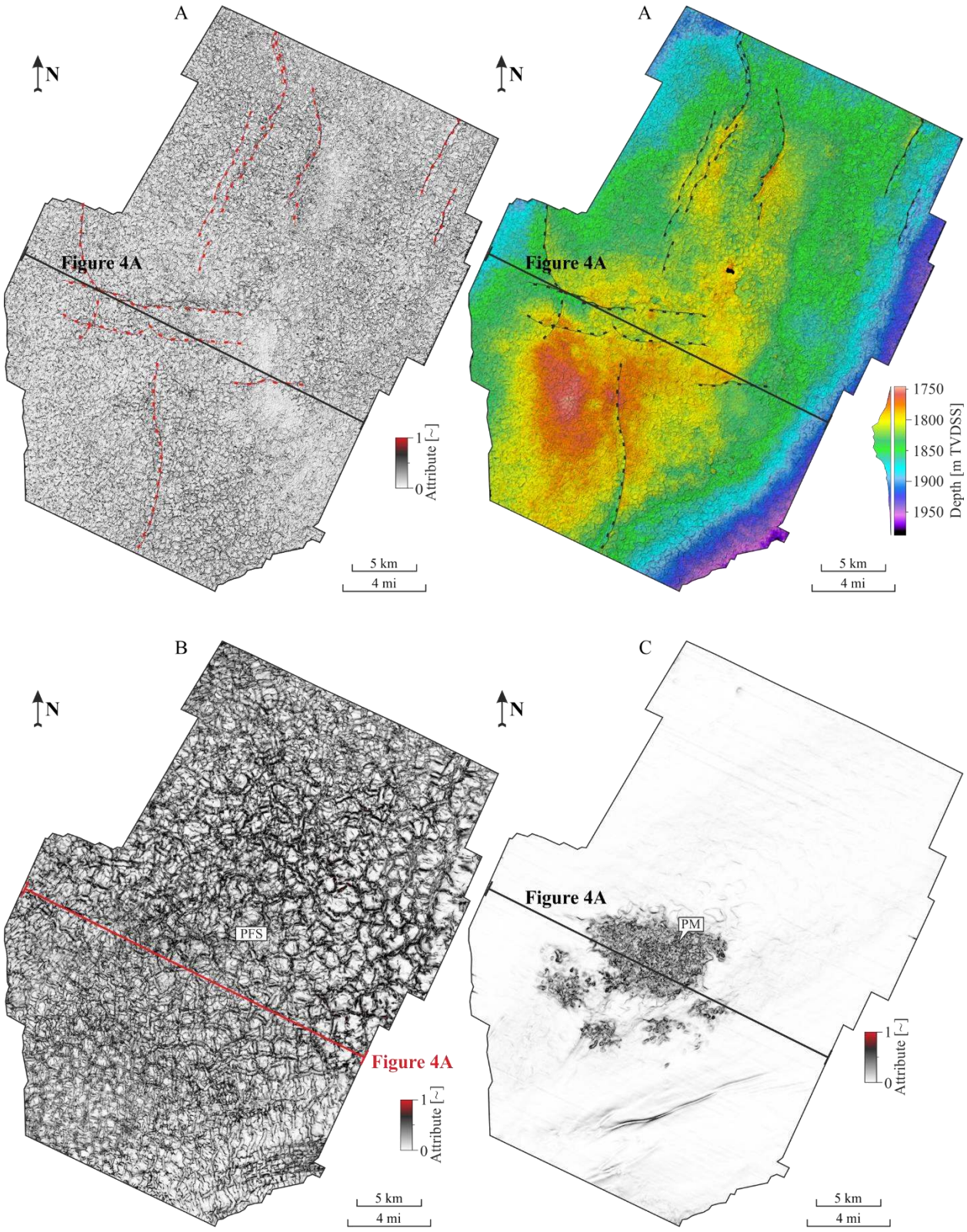

741

742

743 **FIGURE 4**

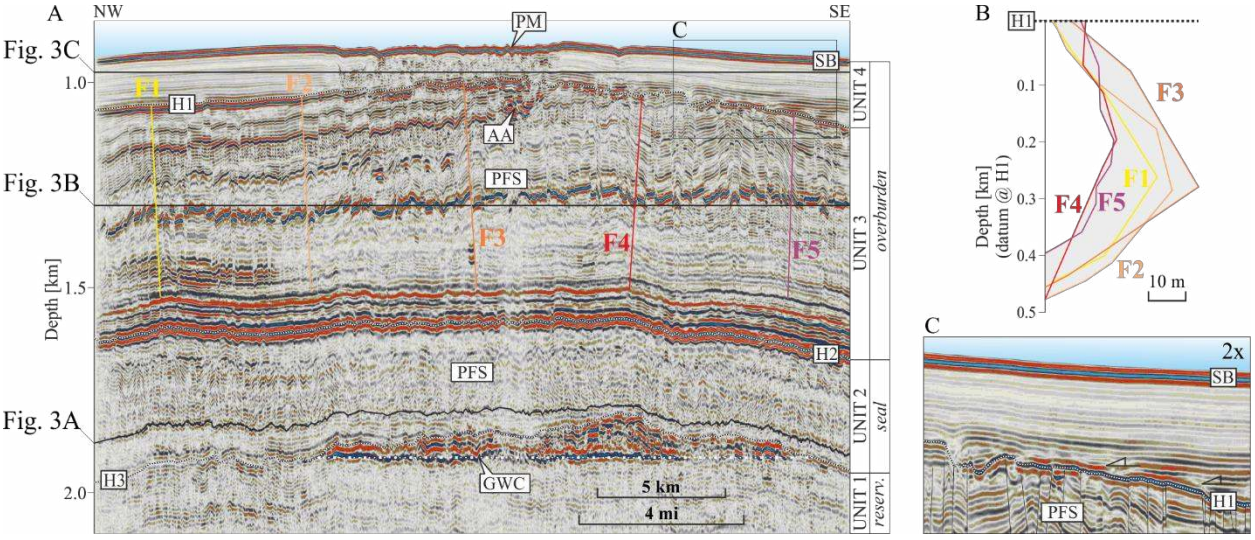

744

745

FIGURE 5

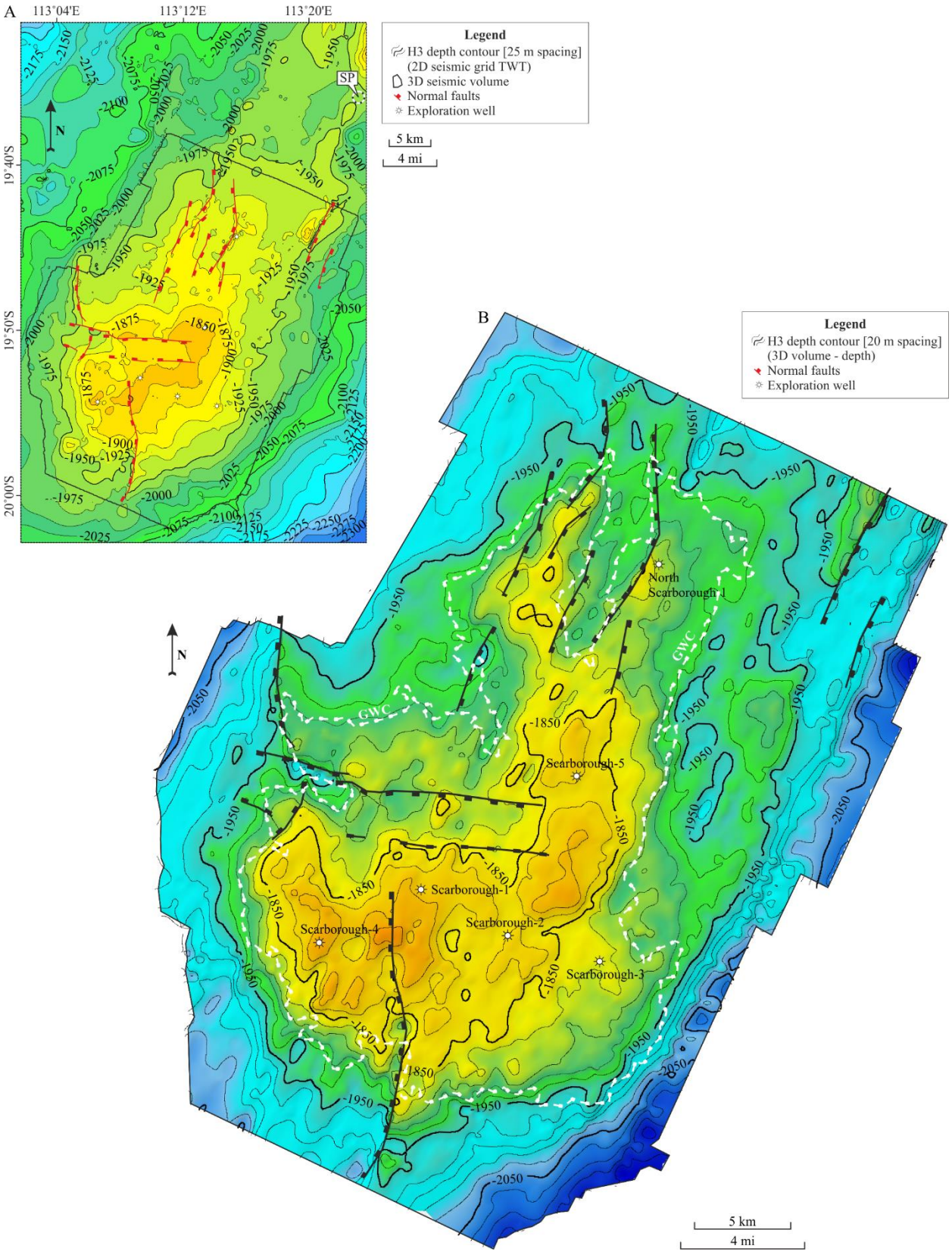
A
113°04'E
113°12'E
113°20'E
19°40'S
19°50'S
20°00'S
N
SP
Legend
H3 depth contour [25 m spacing] (2D seismic grid TWT)
3D seismic volume
Normal faults
Exploration well
5 km
4 mi
B
Legend
H3 depth contour [20 m spacing] (3D volume - depth)
Normal faults
Exploration well
North Scarborough-1
GWC
Scarborough-5
Scarborough-1
Scarborough-2
Scarborough-3
Scarborough-4
5 km
4 mi

748 **FIGURE 6**

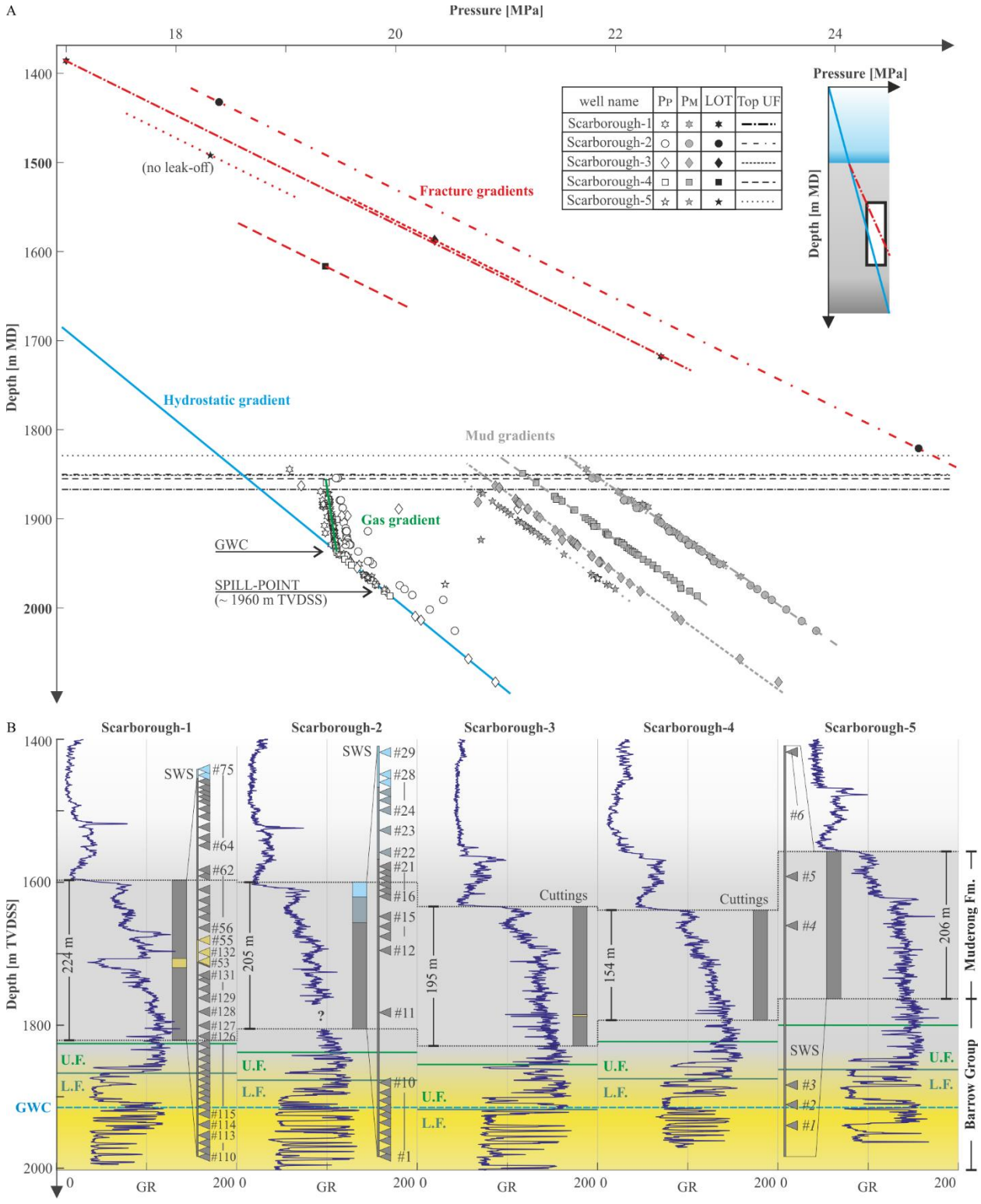

749

750

751 **FIGURE 7**

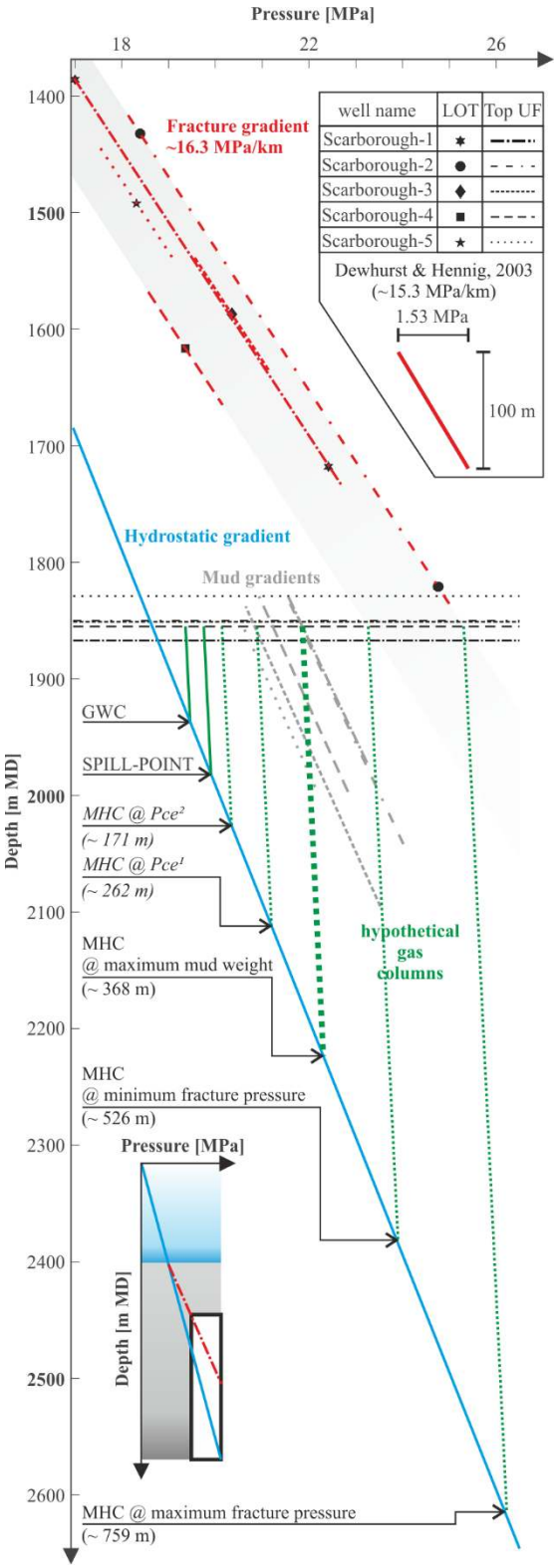

752

753 **FIGURE 8**

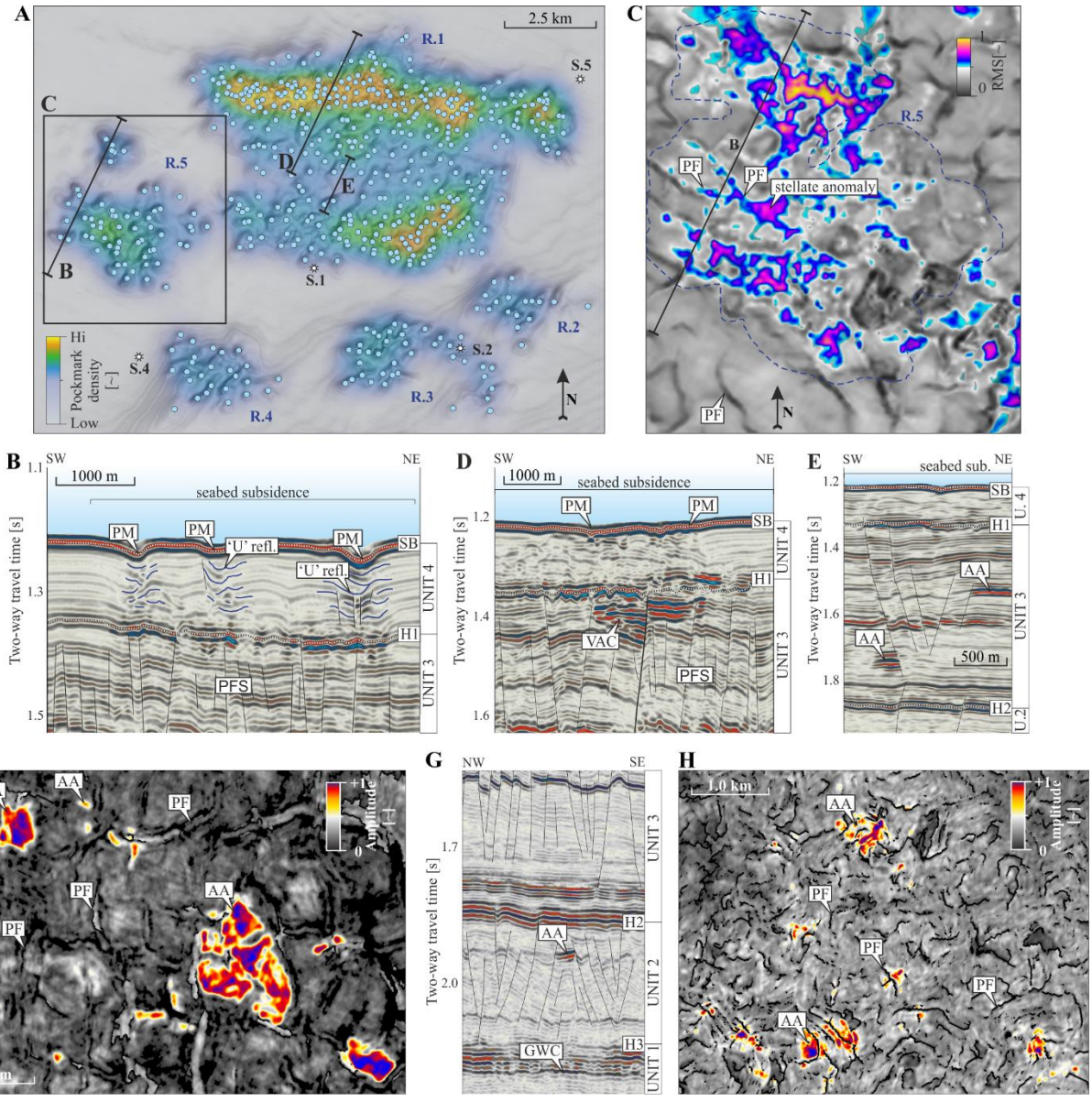
A
2.5 km
R.1
S.5
C
R.5
D
E
B
S.1
R.2
S.2
Hi
Pockmark density [–]
Low
S.4
R.3
R.4
N
C
RMS [–]
0
R.5
B
PF
PF
stellate anomaly
PF
N
B
SW
NE
1000 m
seabed subsidence
PM
PM
'U' refl.
PM
SB
'U' refl.
H1
PFS
UNIT 4
UNIT 3
Two-way travel time [s]
1.1
1.3
1.5
D
SW
NE
1000 m
seabed subsidence
PM
PM
SB
H1
VAC
PFS
UNIT 4
UNIT 3
Two-way travel time [s]
1.2
1.4
1.6
E
SW
seabed sub.
NE
SB
H1
AA
AA
500 m
H2
U. 4
UNIT 3
U.2
Two-way travel time [s]
1.2
1.4
1.6
1.8
F
AA
AA
PF
PF
PF
AA
1 km
+1
Amplitude [–]
0
G
NW
SE
H2
AA
GWC
H3
UNIT 3
UNIT 2
UNIT 1
Two-way travel time [s]
1.7
2.0
H
1.0 km
AA
PF
PF
PF
AA
+1
Amplitude [–]
0

754

755

FIGURE 9

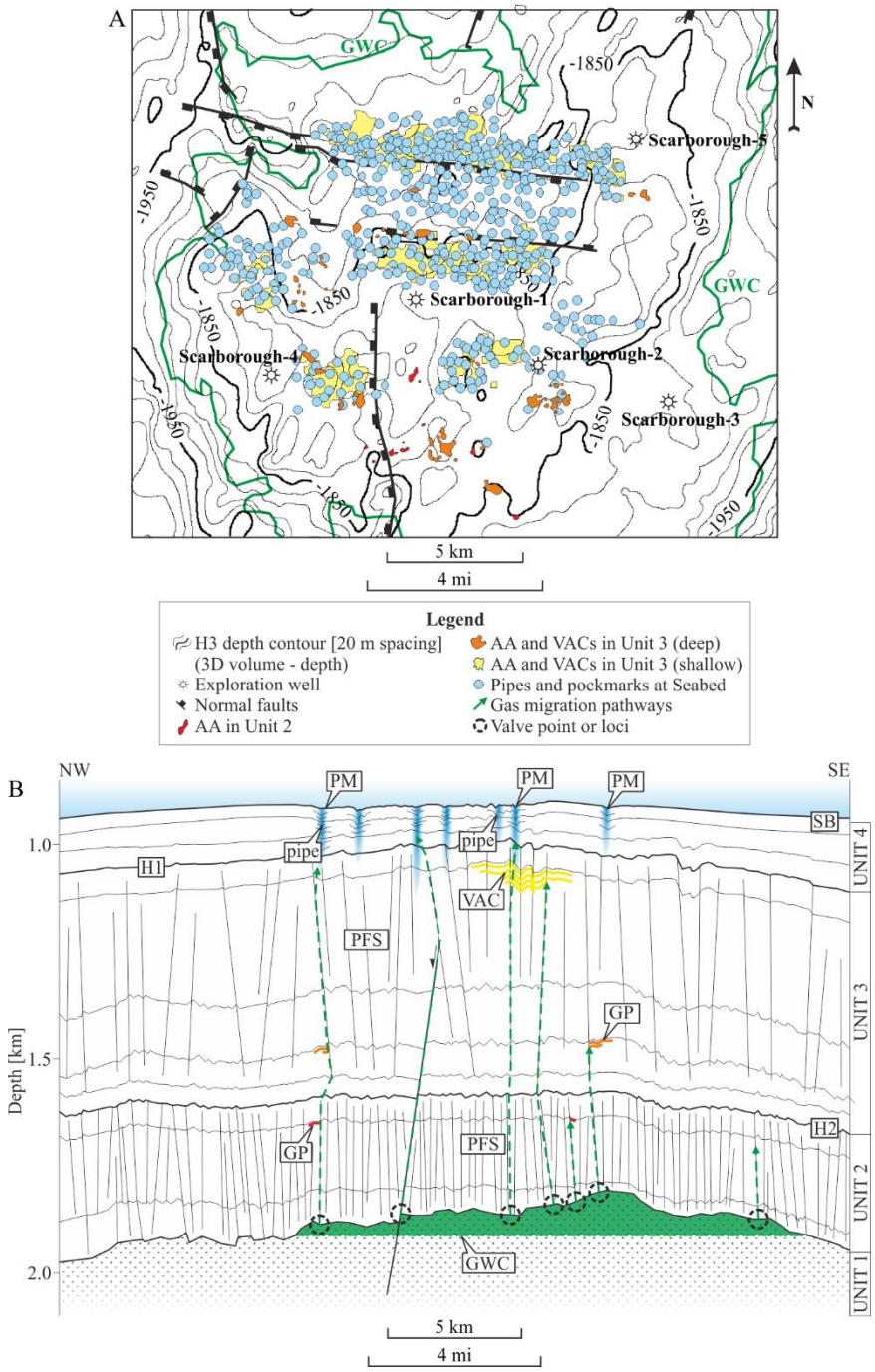
A
GWC
-1850
N
Scarborough-5
-1950
-1850
GWC
-1850
Scarborough-1
Scarborough-4
Scarborough-2
Scarborough-3
-1850
-1950
-1850
-1950
5 km
4 mi
Legend
H3 depth contour [20 m spacing] (3D volume - depth)
Exploration well
Normal faults
AA in Unit 2
AA and VACs in Unit 3 (deep)
AA and VACs in Unit 3 (shallow)
Pipes and pockmarks at Seabed
Gas migration pathways
Valve point or loci
B
NW
SE
PM
PM
PM
SB
pipe
pipe
H1
VAC
PFS
GP
GP
PFS
H2
GWC
UNIT 4
UNIT 3
UNIT 2
UNIT 1
Depth [km]
1.0
1.5
2.0
5 km
4 mi

759 **FIGURE 10**

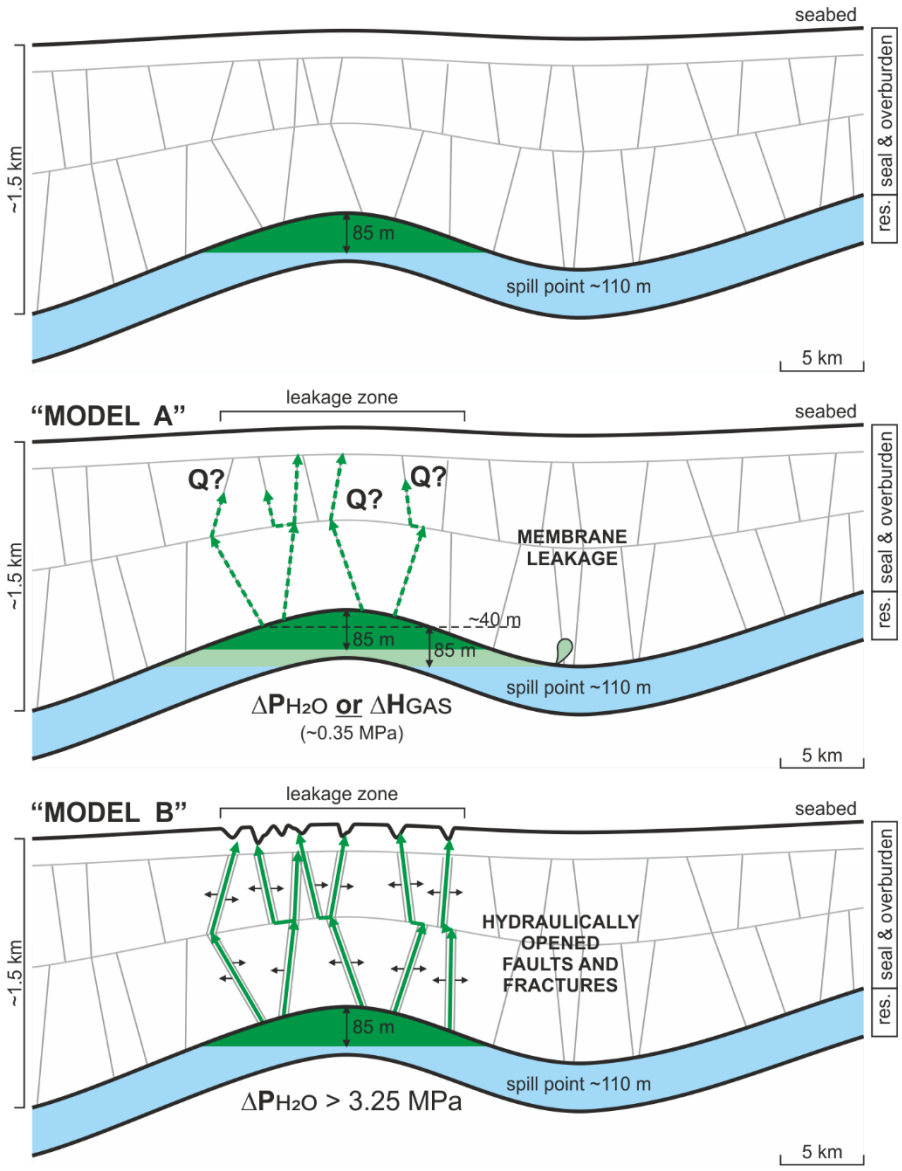

760

761